

Mass of the black hole in the Seyfert 1.5 galaxy H 0507+164 from reverberation mapping

C. S. Stalin,^{1*} S. Jeyakumar,² R. Coziol,² R. S. Pawase³ and S. S. Thakur⁴

¹Indian Institute of Astrophysics, Block II, Koramangala, Bangalore 560 034, India

²Departamento de Astronomia, Universidad de Guanajuato, Guanajuato, CP36000, Mexico

³Laboratoire d'Astrophysique, Ecole Polytechnique Fédérale de Lausanne (EPFL), Observatoire de Sauverny, CH-1290 Versoix, Switzerland

⁴Behind BSF Complex, Paloura Top, Jammu 181124, India

Accepted 2011 May 9. Received 2011 May 6; in original form 2010 July 3

ABSTRACT

We present the results of our optical monitoring campaign of the X-ray source H 0507+164, a low-luminosity Seyfert 1.5 galaxy at a redshift $z = 0.018$. Spectroscopic observations were carried out during 22 nights in 2007, from 2007 November 21 to 2007 December 26. Photometric observations in the R band for 13 nights were also obtained during the same period. The continuum and broad-line fluxes of the galaxy were found to vary during our monitoring period. The R -band differential light curve with respect to a companion star also shows a similar variability. Using cross-correlation analysis, we estimated a time-delay of $\tau_{\text{cen}} = 3.01^{+0.42}_{-1.84}$ d (in the rest frame) of the response of the broad $H\beta$ line fluxes to the variations in the optical continuum at 5100 Å. Using this time-delay and the width of the $H\beta$ line, we estimated the radius for the broad-line region of $2.53^{+0.35}_{-1.55} \times 10^{-3}$ pc and a black hole mass of $9.62^{+0.33}_{-3.73} \times 10^6 M_{\odot}$.

Key words: galaxies: active – galaxies: individual: H 0507+164 – galaxies: Seyfert.

1 INTRODUCTION

The accretion of gas on to a supermassive black hole (SMBH) in the nucleus of galaxies is believed to be the source of activity in quasars and Seyfert galaxies [commonly known as active galactic nuclei (AGNs); cf. Rees 1984]. Several studies have suggested that the mass of the SMBH in these objects is correlated with the luminosity, mass and velocity dispersion of the stellar spheroid of the galaxies (Kormendy & Richstone 1995; Magorrian et al. 1998; Ferrarese & Merritt 2000; Gebhardt et al. 2000; Marconi & Hunt 2003; Häring & Rix 2004). Such correlations may imply an evolutionary relation between the growth of the SMBH and the host galaxy itself (e.g. Somerville et al. 2008; Hopkins & Hernquist 2009; Shankar, Weinberg & Miralda Escudé 2009). In order to study the dependence of the various observed phenomena of AGNs on the black hole mass and the cosmic evolution of the black holes, independent and reliable estimates of the mass of the black holes are required (e.g. Rafter, Crenshaw & Wiita 2009; Goulding et al. 2010).

One independent method to estimate the mass of the black hole is using the reverberation mapping technique (Blandford & McKee 1982; Peterson 1993). In the optical bands, the continuum flux of some AGNs is known to vary on time-scales as short as hours

(e.g. Miller, Carini & Goodrich 1989; Stalin et al. 2004). If the main source of the ionization of the broad-line region (BLR) is the continuum itself, any variation in the continuum emission can also be seen in the broad emission lines. However, the variations in the broad-line flux will have a time-lag (τ) relative to the continuum variations, which can be interpreted as the light traveltime across the BLR. As a first approximation, therefore, the size of the BLR is $R_{\text{BLR}} \leq c\tau$, where c is the velocity of light. Once R_{BLR} is obtained, the mass of the black hole can also be estimated, using the velocity dispersion of the broad component of the emission lines, σ_{line} , and assuming virial equilibrium (Peterson et al. 2004, hereinafter P04; see Peterson 2010, for a recent review).

The reverberation mapping technique has been used to make estimates of SMBH masses over a large range of redshift. However, because the technique is observationally taxing, as it demands an enormous amount of telescope time, to date, the BLR radii of only about three dozen AGNs (Seyfert 1 galaxies and quasars) have been determined (P04; Kaspi et al. 2007; Bentz et al. 2009a; Denney et al. 2009, 2010). Nevertheless, using these estimates, a correlation was found between R_{BLR} and the optical continuum luminosity at 5100 Å (Kaspi et al. 2000; P04; Kaspi et al. 2007; Bentz et al. 2009b; Denney et al. 2009). The $R_{\text{BLR}}-\lambda L_{5100\text{Å}}$ relation can be considered well constrained between the luminosities $10^{43} < \lambda L_{5100\text{Å}} < 10^{45}$ erg s^{-1} . On the other hand, for luminosities below 10^{43} erg s^{-1} , only a handful of sources are observed, and the estimated values of R_{BLR} could also indicate a flattening of the relation (see fig. 2 of Kaspi

*E-mail: stalin@iiap.res.in

et al. 2005). This flattening would suggest a lower limit in the possible masses of SMBHs in galaxies. Although recent revisions of a few sources made by Bentz et al. (2006) and Denney et al. (2009, 2010) are consistent with a continuation of the $R_{\text{BLR}}-\lambda L_{5100\text{\AA}}$ relation to lower luminosities, and consequently with no lower limit in the mass for the SMBH, the correlation is still sparsely sampled. Moreover, the $R_{\text{BLR}}-\lambda L_{5100\text{\AA}}$ relation is very useful for estimating the SMBH masses from single-epoch spectra and calibrating other surrogate relations used for black hole mass estimates (Vestergaard 2004; Shen et al. 2008). Therefore, estimates of R_{BLR} for a larger number of sources are required.

The extrapolation of the known $R_{\text{BLR}}-\lambda L_{5100\text{\AA}}$ relation to low luminosities suggests that the time-lag between the variations of the broad line and that of the continuum will be of the order of hours to days, as compared to several months for high-luminosity sources. Thus, monitoring programmes of short durations, but fast sampling, are required to estimate the reverberation time lags for low-luminosity sources.

In this paper, we present the optical, spectroscopic and photometric observations of a new low-luminosity AGN, the X-ray source and Seyfert 1.5 galaxy H 0507+164. Based on a reverberation mapping campaign that lasted for about a month, during 2007 November–December, we have obtained R_{BLR} and estimated the mass of the SMBH. In Section 2, the observations and data reductions are described. The results of the analysis are given in Section 3, and the conclusions are presented in Section 4.

2 OBSERVATIONS AND REDUCTIONS

Using the Catalogue of Quasars and Active Galactic Nuclei by Véron-Cetty & Véron (12th edn.; Véron-Cetty & Véron 2006), we have compiled a list of nearby Seyfert 1 galaxies, which, based on the available spectra, have a luminosity at $\lambda = 5100\text{\AA}$ of the order of $10^{42}\text{ erg s}^{-1}$ or lower. Very few candidates were found (mostly because of the absence of available spectra). The source, H 0507+164, that we selected for our campaign is identified in the catalogue of Véron-Cetty & Véron as an X-ray source, with coordinates $\alpha_{2000} = 05^{\text{h}}10^{\text{m}}45^{\text{s}}.5$, $\delta_{2000} = 16^{\text{d}}29^{\text{m}}56^{\text{s}}$, and is classified as a Seyfert 1.5 galaxy at a redshift of $z = 0.018$.

Optical, spectroscopic and photometric observations of H 0507+164 were carried out in 2007 between November 21 and December 26 at the 2-m Himalayan Chandra Telescope, operated by the Indian Institute of Astrophysics, Bangalore. The telescope is equipped with a 2048×4096 CCD, coupled to the Himalayan Faint Object Spectrograph and Camera (HFOSC).¹ In imaging mode, only the central 2048×2048 pixels region of the CCD is used. The camera has a plate scale of $0.296\text{ arcsec pixel}^{-1}$, which yields a field of view of $10 \times 10\text{ arcmin}^2$.

2.1 Spectroscopy

Medium-resolution spectra of the nucleus were obtained using a $11\text{ arcmin} \times 1.92\text{ arcsec}$ wide slit and a grism. The spectra have a spectral range of $3800\text{--}6700\text{\AA}$ with a resolution of $\sim 8\text{\AA}$. The exposure time varied between 900 and 1000 s. The spectra were reduced using standard procedures in IRAF.² After bias subtraction

and flat-fielding, one-dimensional spectra were extracted and calibrated, in wavelength using an FeAr lamp and in flux using various observations of the spectrophotometric standard star Feige 34. Since the observed spectra were of low signal-to-noise ratio, for further analysis, all the spectra were smoothed to a resolution of $\sim 15\text{\AA}$.

The standard technique of spectral flux calibration is not sufficiently precise to study the variability of AGNs. Since even under good photometric conditions the accuracy of spectrophotometry is not better than 10 per cent (Shapovalova et al. 2008), we used a relative calibration procedure. A first-order flux calibration was first obtained in the normal way using the standard star. Then, all the spectra were intercalibrated relative to the spectra of one night (we choose November 21), assuming the flux of the narrow line [O III] $\lambda 5007\text{\AA}$ is constant. This is justified, because the narrow-line region (NLR) is much more extended (of the order of a few hundred parsecs) than the BLR (much less than a parsec), and flux variation cannot be observed in this region over short time-scales (cf. Osterbrock 1989). Each spectrum was scaled relative to the reference spectra using the scaling algorithm devised by van Groningen & Wanders (1992). This algorithm uses a chi-square, to minimize the residuals of the [O III] $\lambda 5007\text{\AA}$ line after subtraction from the reference spectrum. The mean spectrum, averaging the spectra of the 22 nights of observations, is shown in Fig. 1.

2.2 Photometry

In parallel to the spectroscopic observations, *R*-band images were also obtained with the HFOSC. Unfortunately, some observations turned out to be contaminated by the light of the extremely bright stars located near the source. As a consequence, our *R*-band photometry covered only 13 of the 22 nights of the campaign. The images were bias subtracted and flat-fielded using IRAF packages. For the rest of the reduction, calibration and analysis, packages in MIDAS³ were used. After removing the cosmic rays, profile-fitting photometry was done using the DAOPHOT and ALLSTAR packages. The observed *R*-band frame is shown in Fig. 2.

3 ANALYSIS

3.1 Light curves

The light curves of the $H\beta$ flux and the continuum at 5100\AA were obtained using the final inter-calibrated spectra. The continuum flux in the rest frame of the galaxy at 5100\AA was obtained using the mean flux within the observed band from $5172\text{--}5200\text{\AA}$.

The $H\beta$ emission-line fluxes were obtained by integrating the emission profile in the band spanning $4884\text{--}5012\text{\AA}$, after subtracting a continuum. An average of the mean fluxes in the regions on the blue ($4808\text{--}4852\text{\AA}$) and red ($5012\text{--}5024\text{\AA}$) sides of the $H\beta$ line was used as the continuum below the line. Although the measured line fluxes include both the narrow and broad components, any variation observed in the line fluxes can be attributed to the broad component only, since the narrow component is not expected to vary during the period of our observations. The light curves for the continuum at 5100\AA , for the $H\beta$ and for the [O III] $\lambda 5007\text{\AA}$ lines are shown in Fig. 3. The corresponding fluxes for the continuum

¹ http://www.iiap.res.in/jao_hfosc

² IRAF stands for Image Reduction and Analysis Facility and is distributed by the National Optical Astronomy Observatories, which is operated by the

Association of Universities for Research in Astronomy, Inc., under contract to the National Science Foundation.

³ Munich Image Data Analysis System; trademark of the European Southern Observatory.

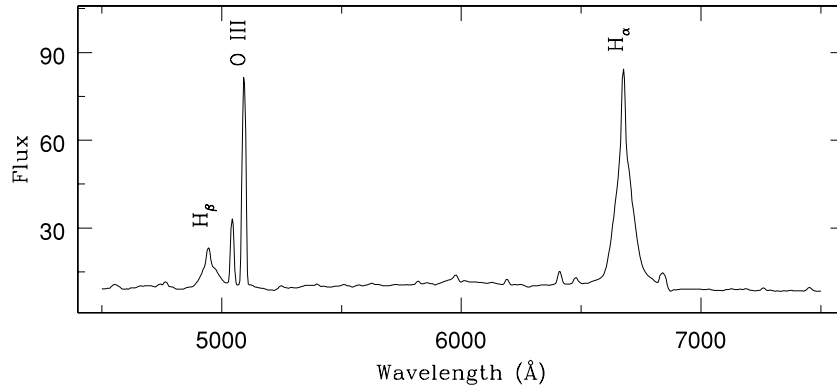


Figure 1. Average spectrum of H 0507+164 obtained by averaging the observations of the 22 nights. The flux is in units of 10^{-16} erg cm^{-2} s^{-1} \AA^{-1} . The classification as Seyfert 1.5 is confirmed, as one can see both a broad and a narrow component for the $\text{H}\beta$ line at $\lambda = 4861$ \AA (cf. Osterbrock 1989).

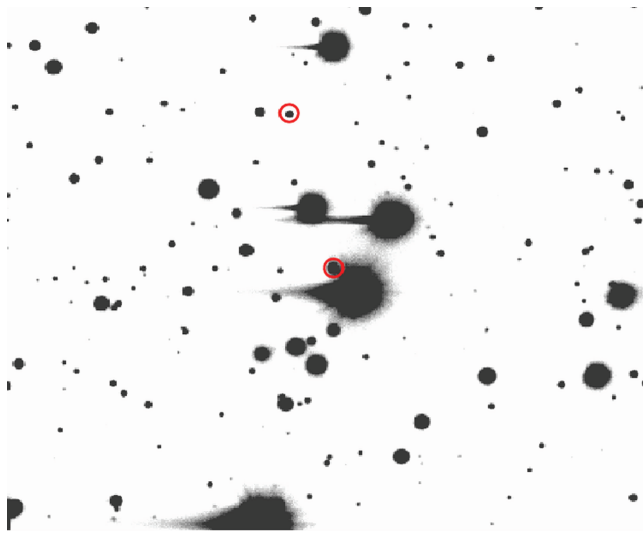


Figure 2. The R -band image of H 0507+164. The galaxy (in the centre) and comparison star (on the top) used for differential photometry are indicated by the circles. The field of view has a dimension of 10×10 arcmin². North is up and east is to the left. Note the presence of an extremely bright star near H 0507+164.

and $\text{H}\beta$ are listed in Table 1. As expected from the intercalibration procedure, the light curve for $[\text{O III}] \lambda 5007$ \AA is nearly constant. On the other hand, both the continuum at 5100 \AA and the $\text{H}\beta$ flux are observed to vary.

The observed R -band differential instrumental magnitudes between the galaxy and the comparison star (marked in Fig. 3) are also given in Table 1. The R -band differential light curve plotted in Fig. 3 (top panel) closely follows the light curves of the continuum at 5100 \AA and $\text{H}\beta$. The average flux at 5100 \AA is $9.03 \pm 1.47 \times 10^{-16}$ erg cm^{-2} s^{-1} \AA^{-1} , which corresponds to $\lambda L_{5100 \text{\AA}}$ of $3.4 \pm 0.55 \times 10^{42}$ erg s^{-1} , for the cosmological parameters $H_0 = 70$ km s^{-1} Mpc⁻¹, $\Omega_m = 0.3$ and $\Omega_\lambda = 0.7$.

The variability of the light curves is characterized by the parameters excess variance, F_{var} , and the ratio between the maximum and minimum flux of the light curves, R_{max} (Rodríguez-Pascual et al. 1997; Edelson et al. 2002). The continuum and $\text{H}\beta$ line have F_{var} of 0.16 and 0.18, and R_{max} of 1.9 ± 0.020 and 1.8 ± 0.016 , respectively. These values are within the range of values found by other variability studies of AGNs (cf. P04; Denney et al. 2010).

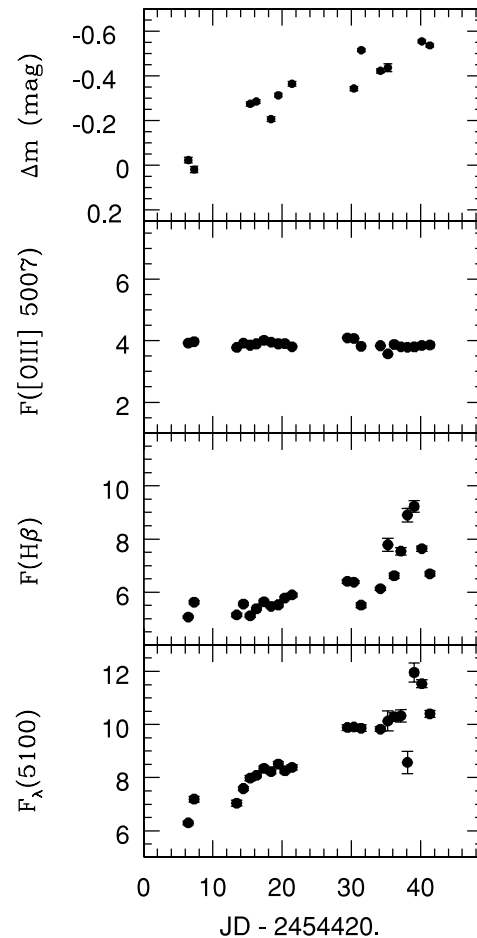


Figure 3. The R -band differential light curve (top panel) and the light curves for $[\text{O III}] \lambda 5007$ \AA , $\text{H}\beta$ and continuum at 5100 \AA are plotted. The fluxes are in units of 10^{-13} erg s^{-1} cm^{-2} \AA^{-1} for the $[\text{O III}] \lambda 5007$ \AA line, 10^{-14} erg s^{-1} cm^{-2} \AA^{-1} for the $\text{H}\beta$ line and 10^{-16} erg s^{-1} cm^{-2} \AA^{-1} for the continuum.

3.2 Time-lag

The time-lag between the variations in the continuum flux and the variations in the $\text{H}\beta$ emission can be determined by cross-correlating the two light curves. For cross-correlation analysis, the method of the interpolated cross-correlation function (ICCF; Gaskell & Sparke 1986; Gaskell & Peterson 1987) and the method

Table 1. Continuum and H β fluxes for the source H 0507+164.

Julian date	$F_{\lambda} \times 10^{-16}$ (5100 Å) (erg s $^{-1}$ cm $^{-2}$ Å $^{-1}$)	H $\beta \times 10^{-14}$ (4861 Å) (erg s $^{-1}$ cm $^{-2}$ Å $^{-1}$)	Δm (mag)
-245 4420			
6.434	6.30 \pm 0.07	5.07 \pm 0.05	-0.022 \pm 0.012
7.289	7.19 \pm 0.10	5.62 \pm 0.07	0.020 \pm 0.015
13.429	7.04 \pm 0.11	5.14 \pm 0.07	
14.389	7.59 \pm 0.07	5.56 \pm 0.05	
15.375	7.98 \pm 0.09	5.11 \pm 0.06	-0.274 \pm 0.009
16.281	8.08 \pm 0.06	5.37 \pm 0.05	-0.285 \pm 0.008
17.376	8.35 \pm 0.08	5.64 \pm 0.05	
18.391	8.22 \pm 0.07	5.47 \pm 0.05	-0.206 \pm 0.010
19.442	8.51 \pm 0.09	5.52 \pm 0.06	-0.313 \pm 0.007
20.391	8.26 \pm 0.07	5.78 \pm 0.05	
21.421	8.39 \pm 0.09	5.90 \pm 0.07	-0.364 \pm 0.010
29.423	9.88 \pm 0.10	6.41 \pm 0.07	
30.366	9.90 \pm 0.08	6.38 \pm 0.06	-0.343 \pm 0.009
31.416	9.86 \pm 0.13	5.51 \pm 0.09	-0.515 \pm 0.006
34.183	9.83 \pm 0.09	6.13 \pm 0.06	-0.422 \pm 0.009
35.257	10.13 \pm 0.37	7.78 \pm 0.24	-0.437 \pm 0.018
36.185	10.30 \pm 0.15	6.62 \pm 0.10	
37.146	10.33 \pm 0.23	7.54 \pm 0.14	
38.092	8.57 \pm 0.42	8.90 \pm 0.26	
39.075	11.96 \pm 0.36	9.23 \pm 0.22	
40.167	11.53 \pm 0.15	7.64 \pm 0.10	-0.554 \pm 0.007
41.326	10.40 \pm 0.13	6.69 \pm 0.08	-0.536 \pm 0.008

of the discrete correlation function (DCF; Edelson & Krolik 1998) were used. Although both the ICCF and DCF methods produce similar results (White & Peterson 1994), the interpolation of the light curve during the period of gaps required by the ICCF method might not be a reasonable approximation to the behaviour of the light curves. Thus, the DCF method is preferable for data with large gaps (Denney et al. 2009). For comparison, we obtain the results using both the methods.

The results of the cross-correlation analysis are shown in Fig. 4. The cross-correlation function (CCF) obtained using the ICCF method is plotted as a thick solid line. The autocorrelation functions (ACFs) of the continuum at 5100 Å and the H β line are also shown in Fig. 4 as the dashed and dotted lines, respectively. For comparison, the CCF obtained using the DCF method is also plotted as a thin solid line. As expected, the autocorrelations have zero time-lags. On the other hand, the time-lag in the cross-correlation curve is clearly notable as an overall shift to the right-hand side. The position of the maximum in the CCF provides an estimate of the time-lag between the continuum and the H β line. The maximum was, however, determined using the centroid, which gives a better estimate for noisy CCFs, rather than the peak, using the formula

$$\tau_{\text{cen}} = \frac{\sum_i \tau_i \text{CCF}_i}{\sum_i \text{CCF}_i}. \quad (1)$$

The estimate of the centroid includes all the points that are within 50 per cent of the peak value of the CCF. Based on this cross-correlation analysis, a statistically significant centroid and the associated uncertainty were obtained using a bootstrap technique that introduces effects of randomness in fluxes and sampling of the light curve (cf. P04). A method to carry out a Monte Carlo simulation using the combined effects of flux randomization (FR) and the random subset selection (RSS) procedures is described in Peterson et al. (1998). Additional improvements as suggested by Welsh (1999) are summarized in P04, which we use for our analysis.

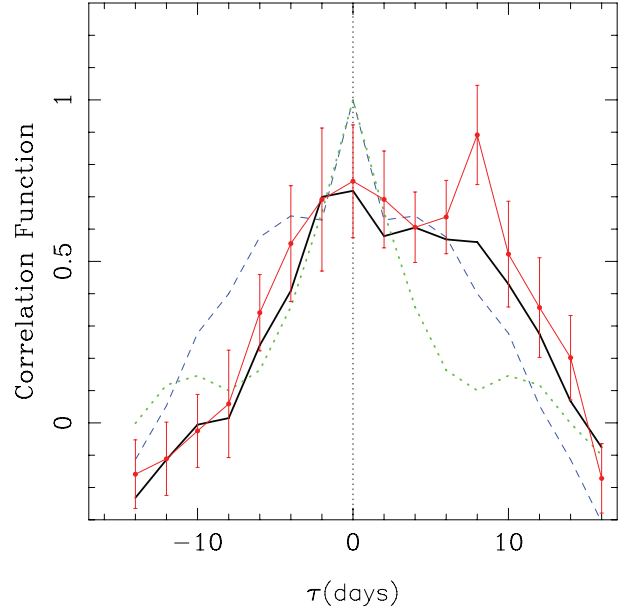


Figure 4. The CCF of the continuum at 5100 Å and the H β light curves, as obtained using the ICCF method, is plotted as the thick solid line. The autocorrelation functions of the continuum at 5100 Å and the H β line are plotted as the dashed and dotted lines, respectively. The CCF obtained using the DCF method is plotted as the thin solid line.

First, a RSS procedure was applied by randomly selecting 22 observations from the light curve. The flux uncertainties of the multiply selected observations were weighted according to Welsh (1999). This light curve was given as input to the FR procedure, where each measured value of the fluxes is modified by adding the measured flux uncertainties multiplied with a random Gaussian value. The modified light curves were then cross-correlated and the centroids were determined as outlined above using CCF values above 50 per cent of the peak value. This procedure was repeated 4000 times, retaining only those CCFs whose maximum

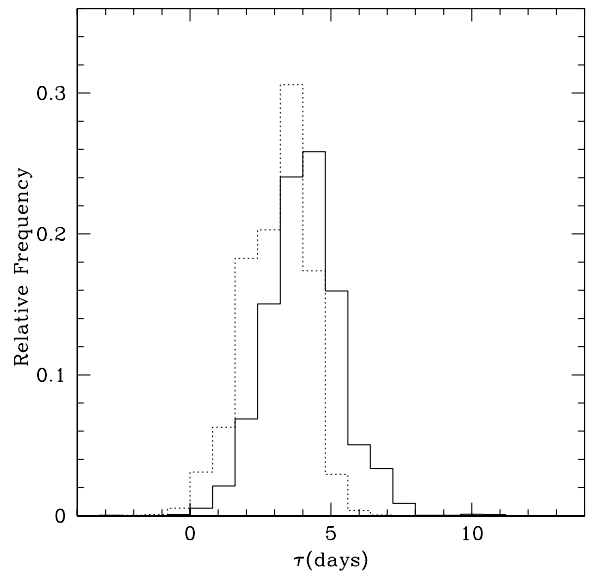


Figure 5. Histogram of the cross-correlation centroids obtained using the FR/RSS realizations. The solid and dotted lines represent the CCCDs determined using the ICCF and DCF, respectively, for a bin size of 2 d.

Table 2. Estimates of centroid values obtained using the DCF and ICCF methods.

Method	Size of the bin (d)				
	2	2.5	3	3.5	4
ICCF	$3.14^{+0.95}_{-1.08}$	$3.28^{+0.67}_{-1.60}$	$3.27^{+0.66}_{-1.64}$	$3.06^{+0.43}_{-1.87}$	$3.05^{+0.40}_{-1.77}$
DCF	$3.91^{+1.30}_{-1.07}$	$4.30^{+1.46}_{-1.44}$	$4.19^{+1.77}_{-0.86}$	$4.11^{+1.19}_{-1.49}$	$4.03^{+0.94}_{-1.40}$

cross-correlation coefficient is large enough such that the correlation is significant with a confidence level of 95 per cent or larger. A cross-correlation centroid distribution (CCCD) was built using the above centroids and is shown in Fig. 5. The average value of the CCCD was taken to be τ_{cent} . Since the CCCD is non-Gaussian (cf. Peterson et al. 1998), the upper and lower uncertainties in τ_{cent} were determined such that 15.87 per cent of CCCD realizations have $\tau > \tau_{\text{cent}} + \Delta\tau_{\text{up}}$ and 15.87 per cent realizations have $\tau < \tau_{\text{cent}} - \Delta\tau_{\text{low}}$. This error in τ_{cent} corresponds to $\pm 1\sigma$ errors for a Gaussian distribution.

The centroid time-lags obtained using different cross-correlation methods for different bin sizes are given in Table 2. The variations due to different bin sizes are within the error bars. The DCF method gives a mean time-lag of about 4 d, whereas the ICCF method gives a mean value of about 3 d. This difference is of the order of the estimated errors on the time-lags. Considering these uncertainties, both the DCF and ICCF methods give time-delays that are consistent with each other. This suggests that the estimated time-lag is not a spurious result for the sampling of the light curves presented here, and the results of the ICCF method are reliable. To be conservative, for further calculations, we use the time-lag with the largest scatter corresponding to a bin size of 3.5 d, obtained using the ICCF method.

Based on this analysis, the average observed-frame time-lag between the H β and the $\lambda = 5100 \text{ \AA}$ continuum light curves was found to be $3.06^{+0.43}_{-1.87}$ d. After correcting for the time-dilation effects using the redshift of the source, we found a time-lag of $3.01^{+0.42}_{-1.84}$ d in the rest frame of the source.

The wavelength coverage of our observations also includes the H α line, and a time-lag using the H α line can also be estimated. However, by repeating the analysis procedure presented here, a reliable time-lag using the H α line could not be found, because the correlation curves are too noisy. This may be due to the shorter duration of the observations and the relative flux calibration procedure

using the [O III] $\lambda 5007 \text{ \AA}$ line situated much farther apart in wavelength from H α being unreliable (Grier et al. 2008). Unfortunately, the nearby doublet [S II] $\lambda\lambda 6716, 6731 \text{ \AA}$ narrow lines, which could be used for the relative calibration of H α , are too weak. Thus, we do not estimate the time-lag using the H α line.

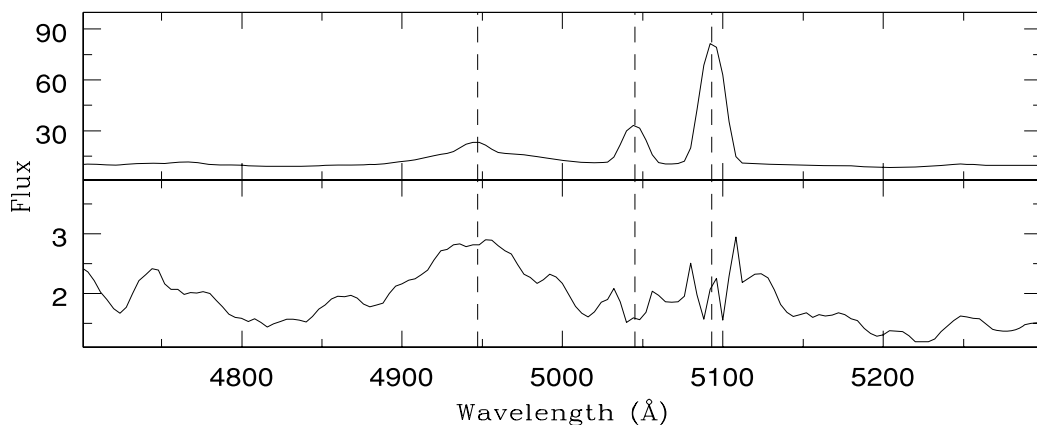
3.3 Linewidth

In order to relate the time-lag to the mass of the black hole, an estimate of the linewidth, the line dispersion σ_{line} , of the broad emission component of H β , is required. Following P04, it is relatively straightforward and more practical to measure σ_{line} , the second moment of the profile, directly from the root-mean-square (rms) spectrum. Indeed, in the rms spectrum, the constant components, or those that vary on time-scales much longer than the duration of the observation, vanish, thus largely obviating the problem of deblending the lines. To obtain the rms spectrum, all the observed spectra were combined using the formula

$$S(\lambda) = \left\{ \frac{1}{N-1} \sum_{i=1}^N [F_i(\lambda) - \bar{F}(\lambda)]^2 \right\}^{1/2}. \quad (2)$$

In Fig. 6, we show the rms spectrum. It can be seen that the two narrow [O III] lines have almost completely disappeared in the rms spectrum.

The mean value of σ_{line} corrected for the instrumental response of the spectrograph and the associated uncertainty were obtained following the bootstrap method described in P04. From our observed 22 observed spectra, we randomly selected 22 spectra, irrespective of whether a particular spectrum had already been selected or not. Since some of the spectra were selected multiple times, the mean value of the resultant number of spectra was smaller by 8. These randomly selected spectra were then used to construct an rms spectrum from which σ_{line} was measured and corrected for the instrumental resolution of the spectrograph. This procedure was repeated 10 000 times, and the mean and standard deviations of these realizations were taken as σ_{line} and its uncertainty, respectively. A distribution of σ_{line} values obtained from the bootstrap method is also shown in Fig. 7. We thus estimate a line dispersion of $\sigma_{\text{line}} = 1725 \pm 105 \text{ km s}^{-1}$.


Figure 6. A zoomed-in version of the mean spectrum (top panel) and corresponding rms spectrum (bottom panel). The flux is in units of $10^{-16} \text{ erg cm}^{-2} \text{ s}^{-1} \text{ \AA}^{-1}$. The rms spectrum shows negligible contribution from the two [O III] narrow lines.

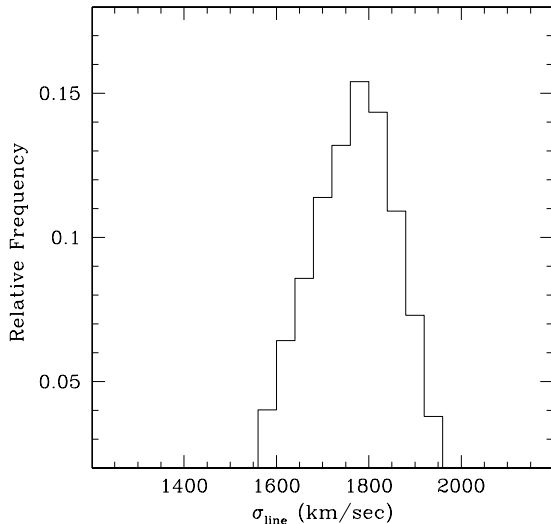


Figure 7. Histogram of the estimates of σ_{line} using the bootstrap method described in the text.

3.4 R_{BLR} and the mass of the black hole

Using the rest-frame time-delay, the radius of the BLR is estimated to be $R_{\text{BLR}} = 2.53^{+0.35}_{-1.55} \times 10^{-3}$ pc. In Fig. 8, we show the measurement of R_{BLR} and $\lambda L_{5100\text{\AA}}$ luminosity of the source presented here along with the most updated data set given by Bentz et al. (2009b) and the additional source, Mrk 290, given by Denney et al. (2010). The solid line is the relation obtained by Bentz et al. (2009b). From this figure, it can be seen that our H β measurement lags are in agreement with the known $R_{\text{BLR}}-L$ relationship.

The mass of the black hole was estimated using the formula in P04:

$$M_{\text{BH}} = f \frac{R_{\text{BLR}} \Delta V^2}{G}, \quad (3)$$

where ΔV is the width of the line and G is the gravitational constant. The parameter f is a scaling factor, which takes into account the geometry and kinematics of the BLR. Onken et al. (2004) found an empirical value of $f = 5.5$, using a sample of AGNs having both reverberation-based black hole masses and host galaxy bulge veloc-

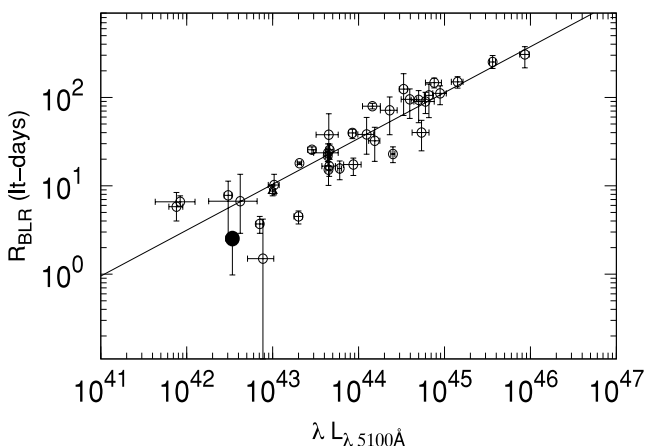


Figure 8. The radius of the BLR versus the continuum luminosity at 5100 Å. The open circles are from Bentz et al. (2009b). The open triangle is the source Mrk 290 reported by Denney et al. 2010. The solid line (with a slope of 0.519) is the fit obtained by Bentz et al. (2009b). The new measurement of this work is shown as a filled circle.

ity dispersion (σ_*) estimates. This value relies on the assumption that both AGNs and quiescent galaxies follow the same $M_{\text{BH}}-\sigma_*$ relationship (Ferrarese & Merritt 2000; Gebhardt et al. 2000). For this particular scaling, the appropriate velocity width ΔV is the line dispersion in the rms spectrum σ_{line} (Bentz et al. 2008). Adopting the Onken et al. (2004) scaling factor and σ_{line} measured from our observations, we estimated the mass of the SMBH in H 0507+164 to be $M_{\text{BH}} = 9.62^{+0.33}_{-3.73} \times 10^6 M_{\odot}$.

4 CONCLUSIONS

We present for the first time monitoring observations of the X-ray source and Seyfert 1.5 galaxy H 0507+164, spanning a time-period of about one month. We have obtained 22 nights of spectra during this period, with a mean sampling time of about 1.6 d. We measured an observed-frame time-lag of about $3.06^{+0.43}_{-1.87}$ d between the changes in the H β emission-line flux and the changes in the continuum flux at $\lambda = 5100$ Å. After correcting for the redshift, we find a corresponding time-lag of $3.01^{+0.42}_{-1.84}$ d in the rest frame of the source. From this measured time-lag, we deduced a size for the BLR of $R_{\text{BLR}} = 2.53^{+0.35}_{-1.55} \times 10^{-3}$ pc and estimated a black hole mass of $9.62^{+0.33}_{-3.73} \times 10^6 M_{\odot}$. Our estimate of R_{BLR} using the measured lag of H β is in agreement with the $R_{\text{BLR}}-\lambda L_{5100\text{\AA}}$ relationship shown by Bentz et al. (2009b).

ACKNOWLEDGMENTS

We thank the anonymous referee for his/her valuable comments that helped to improve the presentation significantly. We also thank B. M. Peterson and R. W. Pogge for kindly providing us with the relative flux scaling program. SJ thanks the grant PROMEP/103-5/07/2462 for partial support. The support provided by the staff at the Indian Astronomical Observatory, Hanle, and CREST, Hoskote, is also acknowledged. This research has made use of the NASA/IPAC Extragalactic Database (NED) which is operated by the Jet Propulsion Laboratory, California Institute of Technology, under contract with the National Aeronautics and Space Administration.

REFERENCES

- Bentz M. C. et al., 2006, ApJ, 651, 775
- Bentz M. C. et al., 2008, ApJ, 689, L21
- Bentz M. C. et al., 2009a, ApJ, 705, 199
- Bentz M. C., Peterson B. M., Netzer H., Pogge R. W., Vestergaard M., 2009b, ApJ, 697, 160
- Blandford R. D., McKee C. F., 1982, ApJ, 255, 419
- Denney K. D. et al., 2009, ApJ, 702, 1353
- Denney K. D. et al., 2010, ApJ, 721, 715
- Edelson R. A., Krolik J. H., 1988, ApJ, 333, 646
- Edelson R., Turner T. J., Pounds K., Vaughan S., Markowitz A., Marshall H., Dobbie P., Warwick R., 2002, ApJ, 568, 610
- Ferrarese L., Merritt D., 2000, ApJ, 539, L9
- Gaskell C. M., Peterson B. M., 1987, ApJS, 65, 1
- Gaskell C. M., Sparke L. S., 1986, ApJ, 305, 175
- Gebhardt K. et al., 2000, ApJ, 539, L13
- Goulding A. D., Alexander D. M., Lehmer B. D., Mullaney J. R., 2010, MNRAS, 406, 597
- Grier C. J. et al., 2008, ApJ, 688, 837
- Häring N., Rix H.-W., 2004, ApJ, 604, L89
- Hopkins P. F., Hernquist L., 2009, ApJ, 694, 599
- Kaspi S., Smith P. S., Netzer H., Maoz D., Jannuzi B. T., Giveon U., 2000, ApJ, 533, 631

- Kaspi S., Maoz D., Netzer H., Peterson B. M., Vestergaard M., Jannuzi B. T., 2005, *ApJ*, 629, 61
- Kaspi S., Brandt W. N., Maoz D., Netzer H., Schneider D. P., Shemmer O., 2007, *ApJ*, 659, 997
- Kormendy J., Richstone D., 1995, *ARA&A*, 33, 581
- Magorrian J. et al., 1998, *AJ*, 115, 2285
- Marconi A., Hunt L. K., 2003, *ApJ*, 589, L21
- Miller H. R., Carini M. T., Goodrich B. D., 1989, *Nat*, 337, 627
- Onken C. A., Ferrarese L., Merritt D., Peterson B. M., Pogge R. W., Vestergaard M., Wandel A., 2004, *ApJ*, 615, 645
- Osterbrock D. E., 1989, *Astrophysics of Gaseous Nebulae and Active Galactic Nuclei*. University Science Books, Mill Valley, CA
- Peterson B. M., 1993, *PASP*, 105, 247
- Peterson B. M., 2010, in Peterson B. M., Somerville R. S., Storchi-Bergmann T., eds, *Proc. IAU Symp. 267, Co-Evolution of Central Black Holes and Galaxies*. Cambridge Univ. Press, Cambridge, p. 151
- Peterson B. M., Wanders I., Horne K., Collier S., Alexander T., Kaspi S., Maoz D., 1998, *PASP*, 110, 660
- Peterson B. M. et al., 2004, *ApJ*, 613, 682 (P04)
- Rafter S. E., Crenshaw D. M., Wiita P. J., 2009, *AJ*, 137, 42
- Rees M. J., 1984, *ARA&A*, 22, 471
- Rodriguez-Pascual P. M. et al., 1997, *ApJS*, 110, 9
- Shankar F., Weinberg D. H., Miralda Escudé J., 2009, *ApJ*, 690, 20
- Shapovalova A. I. et al., 2008, *A&A*, 486, 99
- Shen Y., Greene J. E., Strauss M. A., Richards G. T., Schneider D. P., 2008, *ApJ*, 680, 169
- Somerville R. S., Hopkins P. F., Cox T. J., Robertson B. E., Hernquist L., 2008, *MNRAS*, 391, 481
- Stalin C. S., Gopal-Krishna, Sagar R., Witta P. J., 2004, *JA&A*, 25, 1
- van Groningen E., Wanders I., 1992, *PASP*, 104, 700
- Véron-Cetty M. P., Véron P., 2006, *A&A*, 455, 776
- Vestergaard M., 2004, *ApJ*, 601, 676
- Welsh W. F., 1999, *PASP*, 111, 1347
- White R. J., Peterson B. M., 1994, *PASP*, 106, 879

This paper has been typeset from a $\text{\TeX}/\text{\LaTeX}$ file prepared by the author.